ELSEVIER

Journal of Power Sources 106 (2002) 224–230

JOURNAL OF POWER SOURCES

www.elsevier.com/locate/jpowsour

Imaging of oxygen transport at SOFC cathode/electrolyte interfaces by a novel technique

Teruhisa Horita[a,*], Katsuhiko Yamaji[a], Natsuko Sakai[a], Yueping Xiong[a], Tohru Kato[a], Harumi Yokokawa[a], Tatsuya Kawada[b]

[a]*National Institute of Advanced Industrial Science and Technology (AIST), AIST Tsukuba Central 5, 1-1-1 Higashi, Tsukuba, Ibaraki 305-8565, Japan*

[b]*Tohoku University, Sendai, Japan*

Abstract

Oxygen transport was examined around the O_2/cathode/yttria-stabilized zirconia (YSZ) interfaces in solid oxide fuel cells (SOFCs). To visualize the kinetics of oxygen transport, isotope oxygen exchange ($^{16}O/^{18}O$ exchange) and secondary ion mass spectrometry analysis (SIMS) were adopted for $La_{0.85}Sr_{0.15}MnO_3$-mesh and gold (Au)-mesh cathodes. The mesh cathode surfaces promoted oxygen adsorption and surface oxygen exchange. Oxygen bulk diffusion in the mesh cathode was observed only at the $La_{0.85}Sr_{0.15}MnO_3$-mesh. The active sites for oxygen incorporation were compared at the YSZ surfaces after removing the mesh cathodes. The $La_{0.85}Sr_{0.15}MnO_3$-mesh/YSZ interface can be the active site for oxygen incorporation as well as the triple phase boundary (TPB). On the other hand, the Au/YSZ interface showed low ^{18}O concentration, and the active sites were limited to the TPB lines. Most active sites for oxygen incorporation were the O_2/cathode/YSZ interface (TPB) for $La_{0.85}Sr_{0.15}MnO_3$-mesh and Au-mesh from the line analysis of the SIMS images. The expansion of the oxygen incorporation active site around the TPB was discussed on the basis of SIMS imaging analysis and electrochemical analysis.

Keywords: Oxygen transport; Isotope oxygen exchange; $^{16}O/^{18}O$ exchange; Secondary ion mass spectrometry (SIMS); Cathode reaction

1. Introduction

Oxygen transports is an important phenomenon for solid oxide fuel cells (SOFCs) because it is related to the cathode overpotential (η) at the cathode/electrolyte interfaces. Since the cathode overpotential is one of the major resistances of SOFCs, it must be minimized to improve performance. For minimizing the cathode overpotential, the oxygen transport mechanism should be clarified around the O_2/cathode/electrolyte interfaces. To date, many reports have been published about the oxygen transport mechanism by electrochemical methods [1–22] with changing the oxygen partial pressure, temperature, and applied voltage. The overall oxygen reduction at the O_2/cathode/electrolyte interface can be written in the following equation:

$$\frac{1}{2}O_2 + 2e^- + V_O^{\bullet\bullet} \rightarrow O_O^{\times} \quad (1)$$

where, $V_O^{\bullet\bullet}$ indicates oxygen vacancies in the electrode or the electrolyte. Fig. 1 shows a schematic representation of oxygen reduction around the O_2/cathode/electrolyte interface. The oxygen reduction can be divided into several elemental steps: (1) oxygen dissociate adsorption on cathode surface; (2) surface diffusion of oxygen on the cathode; (3) incorporation of oxygen into electrolyte via the triple phase boundary (TPB); (4) oxide ion diffusion in the bulk of cathode; and (5) oxide ion transfer from cathode to electrolyte. One of these steps can be the rate-determining in the cathodic reaction. According to previous studies, cathode materials can be classified as two types in terms of their oxygen diffusivity in the bulk and the surface oxygen diffusion. The effects of oxygen bulk diffusion on the cathodic reaction have been reported by M. Kleitz and F. Petitbon [7] and E. Siebert and co-workers [8,9]. They have shown oxygen diffusion in silver (Ag) and $LaMnO_3$ under cathodic polarization, and suggested the effects of bulk oxygen diffusion on the cathodic reaction. On the other hand, many authors reported the importance of the TPB area for oxygen reduction in platinum (Pt), gold (Au), and $LaMnO_3$-based cathodes to improve cathode performance. Therefore, the technologically important issue for designing the cathode/electrolyte interface is the expansion of electrochemically active sites around the TPB. Electrochemical

* Corresponding author. Tel.: +81-298-61-4542; fax: +81-298-61-4540.
E-mail address: t.horita@aist.go.jp (T. Horita).

0378-7753/02/$ – see front matter
PII: S0378-7753(01)01017-5

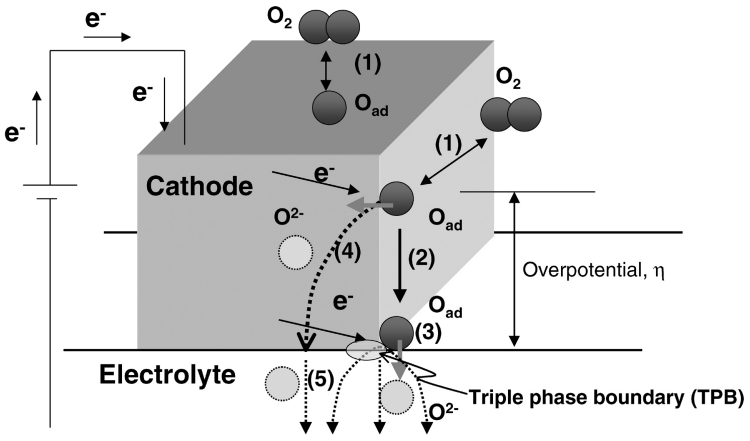

Fig. 1. Schematic representation of oxygen transport around the O_2/cathode/electrolyte interface: (1) oxygen dissociate adsorption on cathode surface; (2) surface diffusion of adsorption oxygen; (3) incorporation of adsorption oxygen via TPB; (4) bulk diffusion of oxygen through cathode; (5) oxide ion transfer at the cathode/electrolyte interface.

analyses suggested some reasonable models for oxygen reduction and/or transports. However, there still remain some unclear points about oxygen transport around O_2/cathode/electrolyte interfaces: (1) activity for oxygen adsorption on cathode surface; (2) diffusivity of oxygen in cathode materials; and (3) active site distribution for oxygen incorporation around the interfaces.

To answer the above questions, we have adopted the stable oxygen isotope ($^{18}O_2$) as a diffusion marker, and applied a secondary ion mass spectrometry (SIMS) technique for imaging the distribution of ^{18}O [23–25]. That is, the dynamics of oxygen transport were observed at the O_2/cathode/electrolyte interfaces (triple phase boundary (TPB)) in the "frozen state" by this novel technique. To define the contact of O_2/electrode/electrolyte precisely, mesh shaped electrodes were prepared on the yttria-stabilized zirconia (YSZ) [25]. In previous reports, oxygen diffusion and the active sites for oxygen reduction were visualized at the (La, Sr) MnO_3 cathode mesh/YSZ interfaces under different cathodic polarizations [26]. We have also shown the bulk diffusion of oxygen under cathodic polarization by this technique [27,28]. However, the effects of the cathode materials on the oxygen transports and the distribution of active sites for oxygen reduction have not been clarified. The aim of this study is, therefore, the clarification of oxygen transport at the different cathode materials on YSZ (cathode; (La, Sr) MnO_3 and Au) for designing the optimum cathode/electrolyte interface structure.

2. Experimental

2.1. Samples

The mesh shape cathodes were prepared by two methods: one is the photolithography technique, and the other is the pressing of the grid mesh on the substrate at high temperature. For preparing the mesh shape $La_{0.9}Sr_{0.1}MnO_3$ cathode, a dense $La_{0.9}Sr_{0.1}MnO_3$ film was firstly formed by the RF-sputtering technique on the Y_2O_3-stabilized ZrO_2 (YSZ, 8 mol%Y_2O_3-doped ZrO_2). During sputtering, the substrate YSZ was annealed at 973 K to prepare a dense homogeneous $La_{0.9}Sr_{0.1}MnO_3$ film. The mesh shape $La_{0.9}Sr_{0.1}MnO_3$ was subsequently prepared by the photolithography techniques on YSZ. For preparing the Au-mesh, a grid mesh in the grade of #200 (JEOL Co. Ltd.) was attached on the YSZ single crystal and fired at high temperature (1283 K for 2 h). Fig. 2 shows scanning electron microscope (SEM) image and optical microscope image of the $La_{0.9}Sr_{0.1}MnO_3$-mesh and the Au-mesh on YSZ substrates, respectively. The images show good contact at the mesh cathode/YSZ interface. It also shows clear boundaries at O_2/the cathode/YSZ interface, at which we can determine the edge of the mesh cathodes on YSZ.

2.2. Isotope oxygen exchange ($^{16}O/^{18}O$ exchange)

The experimental setup is schematically drawn in Fig. 3. The sample was initially annealed in $^{16}O_2$ (purity is 99.99 vol.%) under cathodic polarization in the closed gas-exchanging cell. After annealing in $^{16}O_2$ for more than 1 h, the atmosphere was suddenly switched to $^{18}O_2$, atmosphere under the same cathodic polarization (the concentration of $^{18}O_2$ was above 95%). The duration time for annealing was 600 s at 973 K at $p(O_2) = 0.1$ bar. The voltage was applied in the cathodic direction of from 0 to 0.5 V (up to −0.5 V versus the reference electrode). After $^{16}O/^{18}O$ exchange, the samples were quenched to room temperature in a short duration (973–273 K in 30 s).

2.3. SIMS measurements

The SIMS analysis was conducted with a sector-type instrument (CAMECA ims-5f). A primary Cs^+ beam sputtered

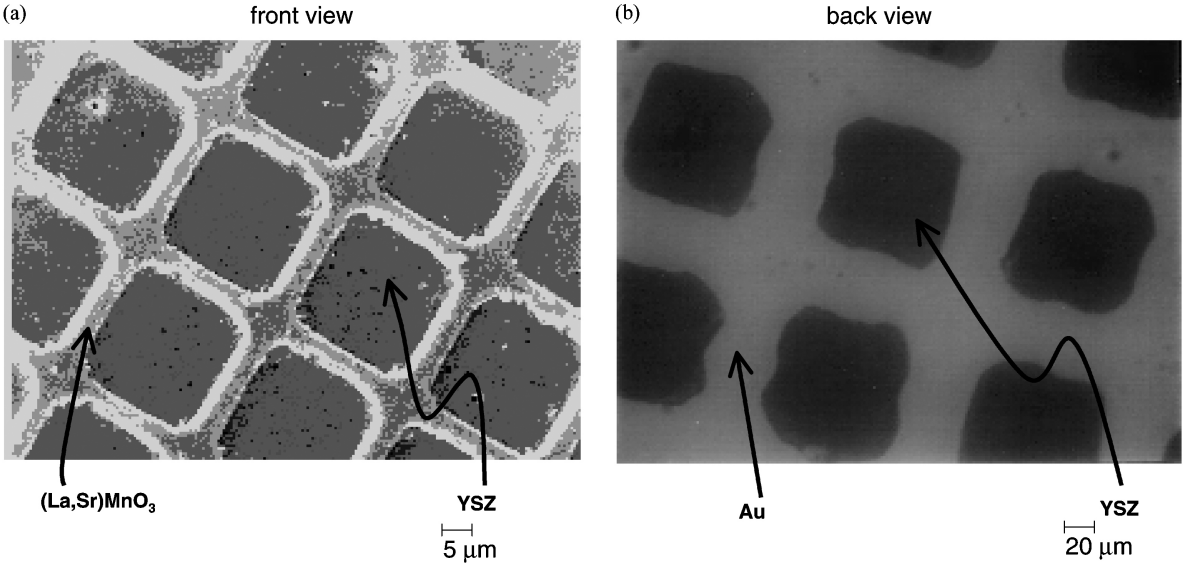

Fig. 2. Microstructures of the mesh cathodes: (a) front view of the $La_{0.9}Sr_{0.1}MnO_3$-mesh/YSZ sample; (b) back view of the Au-mesh/YSZ sample.

the sample surface, and negative secondary ion intensities ($^{16}O^-$, $^{18}O^-$, $Mn^{16}O^-$, $La^{16}O^-$, $Zr^{16}O^-$, and $Y^{16}O^-$) were recorded as a function of the depth. The acceleration voltage was 10 kV, and the primary beam current was 10–50 nA for depth profile analysis. The mass resolution, $M/\Delta M$, was 300 in a normal operation mode. This was enough resolution to distinguish the signal between $^{18}O^-$ and $H_2{}^{16}O^-$. In the imaging mode, the diameter of the primary beam was focused to be about 0.2 μm and the secondary ion images were collected in the area of 30 μm × 30 μm or 150 μm × 150 μm. For insulating materials, on electronic shower was applied to compensate the charge at the sample surface.

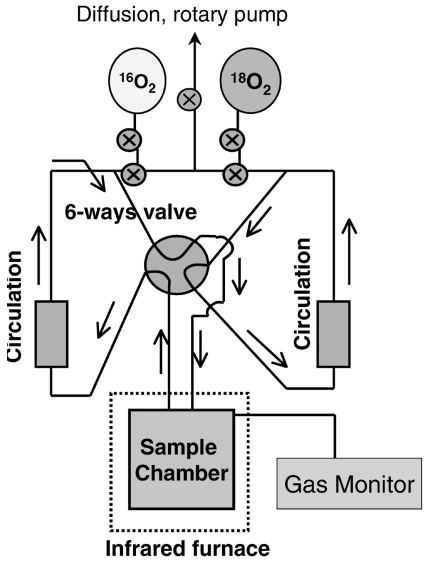

Fig. 3. Schematic diagram of oxygen isotope ($^{16}O_2/^{18}O_2$) exchange equipment.

3. Results and discussion

3.1. Cathodic polarization of the mesh cathode

Fig. 4 shows steady-state cathodic polarization curves of the mesh cathode/YSZ samples at 973 K in the fixed oxygen partial pressure (0.1 bar). The polarization curves of the mesh cathodes show a significant difference in the current density: Au-mesh shows about 1 order of magnitude lower current density than the current density of the $La_{0.9}Sr_{0.1}MnO_3$-mesh at the same overpotential. Also, the polarization curve of $La_{0.9}Sr_{0.1}MnO_3$-mesh shows a significant hysteresis between forward and backward polarization. This phenomenon has often been reported by some authors [17,18], and it can be related to the changes of the oxygen vacancy concentration in the $La_{0.9}Sr_{0.1}MnO_3$-mesh. For the polarization curve of the Au-mesh/YSZ sample, a limiting current is observed at the higher cathodic polarization (higher than −0.1 V). This is due to the limitation of the supply of electrochemically active species, such as adsorption oxygen on the cathode.

The solid lines in the figure show the fitting lines of the Butler–Volmer like equation to the measured data in the range of $-0.1 < \eta < 0$, as follows:

$$J = J^{O}[\exp(n\alpha_a f\eta) - \exp(-n\alpha_c f\eta)] \quad (2)$$

where, J^O is the exchange current density, n the number of electrons (in this case $n = 2$), α the transfer coefficient (in this case, $\alpha_a = \alpha_c = 0.5$), $f = F/RT$, ($F = 96485$ C mol^{-1}, $R = 8.314$ J K^{-1} mol^{-1}, $T = 973$ K), and η is the cathodic overpotential. From the fitting lines, the exchange current density (J^O) was calculated for each electrode. The values obtained are 4×10^{-4} A cm^{-2} for Au-mesh and 1.8×10^{-3} A cm^{-2} for $La_{0.9}Sr_{0.1}MnO_3$-mesh. These values are consistent with the reported values, and the mesh electrodes

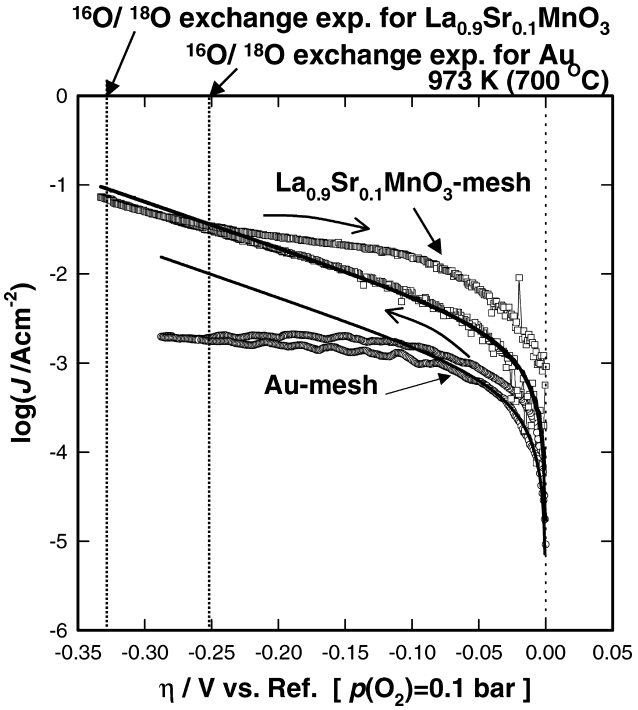

Fig. 4. Steady-state cathodic polarization curves of the $La_{0.9}Sr_{0.1}MnO_3$-mesh/YSZ and the Au-mesh/YSZ at 973 K under $p(O_2) = 0.1$ bar (the broken lines indicate the cathodic overpotentials at which the $^{16}O/^{18}O$ exchange were performed).

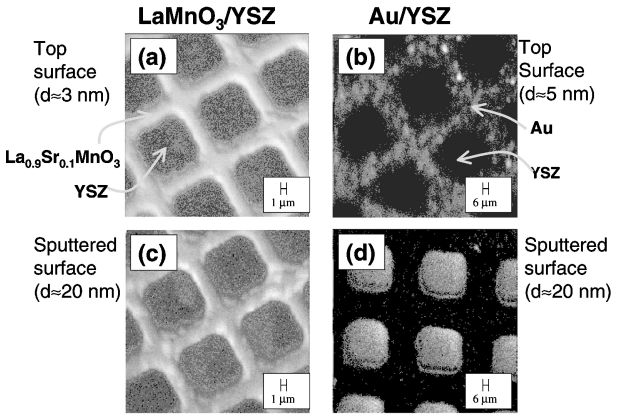

Fig. 5. SIMS images of ^{18}O concentration at the mesh cathode/YSZ interfaces ((a) top surface of the $La_{0.9}Sr_{0.1}MnO_3$-mesh/YSZ; (b) top surface of the Au-mesh/YSZ; (c) sputtered surface of the $La_{0.9}Sr_{0.1}MnO_3$-mesh/YSZ; (d) sputtered surface of the Au-mesh/YSZ.

adopted in this study show similar electrochemical properties to those of normal porous cathodes [1,5]. The isotope oxygen exchange ($^{16}O/^{18}O$ exchange) was conducted at the marked overpotentials: −0.25 V for the Au-mesh, and −0.33 V for the $La_{0.9}Sr_{0.1}MnO_3$-mesh. In the Au-mesh sample, the experimental current density was 2×10^{-3} A cm^{-2}, which corresponds to the ^{18}O concentration of 6×10^{-5} mol cm^{-3} for 600 s. This value is close to the detection limit of SIMS analysis.

3.2. Oxygen adsorption and diffusion on cathode materials

Fig. 5 shows SIMS images of the concentration of ^{18}O for the mesh shape cathodes/YSZ samples. These images are the concentration of $^{18}O^-$ signal $[C(^{18}O) = I(^{18}O^-)/\{I(^{16}O^-) + I(^{18}O^-)\}]$ for each position. The whiter color indicates the higher ^{18}O concentration in these images. At the top surface (Cs^+ sputtering for 10 s, estimated to be 3–5 nm depth, in Fig. 3(a) and (b)), the higher ^{18}O concentration is observed on the mesh parts. This indicates that the mesh cathode surface is more active for oxygen adsorption or oxygen surface exchange than the YSZ surface. On the other hand, the images after sputtering for a prolonged duration show different images (in Fig. 3(c) and (d)): the lower ^{18}O concentration is found to be at the Au-mesh part, though the higher ^{18}O concentration is still observed at the $La_{0.9}Sr_{0.1}MnO_3$-mesh part. The sputtering depths are estimated to be around 20 nm from the surface. Therefore, the diffusion length of ^{18}O is less than 20 nm in Au, and it is longer than 20 nm in the $La_{0.9}Sr_{0.1}MnO_3$-mesh. From these SIMS images, both mesh cathode surfaces are active for oxygen adsorption or isotope oxygen surface exchange ($^{16}O/^{18}O$ exchange). The difference comes from the solubility of oxygen or the diffusivity of oxygen in the bulk of the cathode materials. This difference affects the oxygen transports at the cathode/YSZ interfaces. In the $La_{0.9}Sr_{0.1}MnO_3$ cathode, some amounts of oxygen can diffuse via the oxygen vacancy. However, in the Au cathode, almost no oxygen can diffuse in the Au bulk.

3.3. Incorporation of oxygen at the cathode/YSZ interfaces

In order to clarify the oxygen incorporation active sites, the covered mesh cathodes were removed by chemical etching techniques: the mesh samples were washed by HCl solution or aqua regia. Fig. 6 shows SIMS images of the YSZ surface after removing the mesh cathodes.

For the $La_{0.9}Sr_{0.1}MnO_3$-mesh removed YSZ surface (Fig. 6(a)), a high ^{18}O concentration is observed in the shape of the mesh. These parts correspond to the two-phase contact of $La_{0.9}Sr_{0.1}MnO_3$-mesh/YSZ. Also, many ^{18}O hot spots are observed in the mesh parts. This suggests that the $La_{0.9}Sr_{0.1}MnO_3$ mesh/YSZ interfaces are active for oxygen incorporation, and the active sites are distributed as (many) spots at the interface (not homogeneously distributed at the interface).

For the Au-mesh removed YSZ surface (Fig. 6(b)), a high ^{18}O concentration is found in the shape of a ring with a significant low concentration at the Au/YSZ two-phase boundaries. These high ^{18}O concentration parts correspond to the edge of the mesh. That is, only the interface of O_2/Au-mesh/YSZ (TPB) is active for the oxygen incorporation. A ring shape image suggests that the active sites for oxygen incorporation are within a few μm of the TPB lines, and the blocking of oxygen incorporation at the Au/YSZ interface.

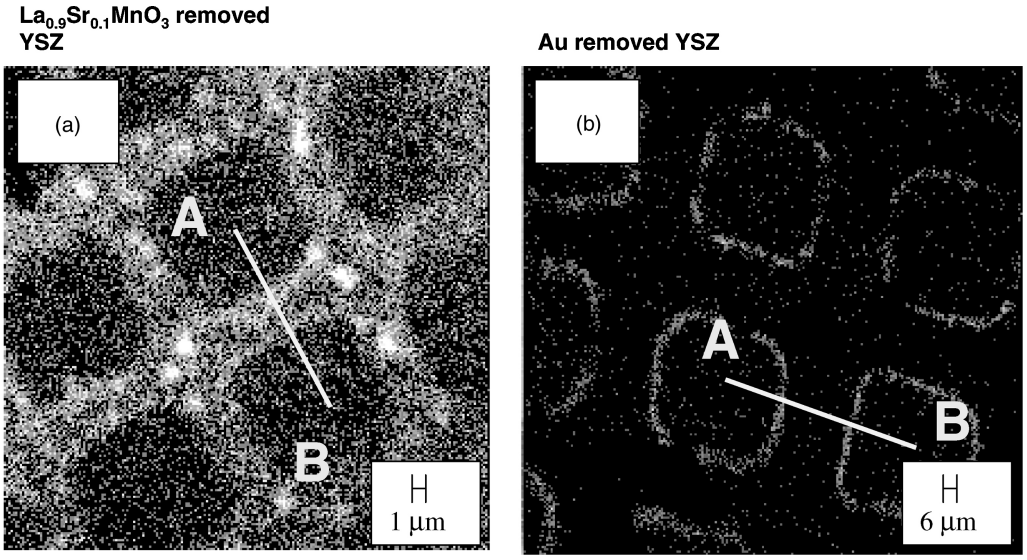

Fig. 6. SIMS images of ^{18}O concentration on the mesh cathode removed YSZ surface: (a) $La_{0.9}Sr_{0.1}MnO_3$-mesh removed YSZ surface; (b) Au-mesh removed YSZ surface.

3.4. Line analysis of the SIMS images

In order to analyze the active sites for ^{18}O incorporation more precisely, a line analysis was examined for the SIMS images of ^{18}O concentration (along the lines in the images between A and B). Fig. 7 shows line analyses of SIMS images at several depths for YSZ after removing the $La_{0.9}Sr_{0.1}MnO_3$-mesh and the Au-mesh cathodes.

For the $La_{0.9}Sr_{0.1}MnO_3$-mesh removed YSZ surface, two peaks of high ^{18}O concentration are identified around the position of $x = 6$ and 8 μm in Fig. 7(a) (at the depth of $d = 3$, 18, and 45 nm). These two peaks are thought to be the active sites for oxygen incorporation on the YSZ surface. The width of the tops of these two peaks is consistent with that of the mesh cathode (about 2 μm). Therefore, the most active sites for oxygen incorporation are around the TPB area, and the active sites do not expand very much from the TPB line. A splitting of two peaks suggests that the active sites expansion is less than 1 μm from the TPB lines. Since the ^{18}O concentration at the $La_{0.9}Sr_{0.1}MnO_3$/YSZ interface ($x = 6-8$ μm in Fig. 7(a)) is higher than at the YSZ free surface ($x < 6$ μm, $x > 8$ μm in Fig. 7(a)), the $La_{0.9}Sr_{0.1}MnO_3$/YSZ interface can also be the active site for oxygen incorporation. At the deeper position of YSZ ($d = 101$ nm), almost no peaks of ^{18}O concentration are observed in the line analysis, which suggests a homogeneous distribution of ^{18}O inside the YSZ.

For the Au-mesh removed YSZ (Fig. 7(b)), the line analysis shows more clearly two peaks of ^{18}O concentration than in the case of the $La_{0.9}Sr_{0.1}MnO_3$-mesh. These two peaks correspond to the edge of the Au-mesh and TPB lines. The width of the top of these two peaks is consistent with that of the Au-mesh. Therefore, the active sites for oxygen incorporation are limited to the narrow zone of TPB lines within a few μm area. With increasing sputtering time (deeper analysis position), the ^{18}O concentration of these two peaks becomes lower than for the surface area.

Due to the difference of the plane resolution of two SIMS images (Fig. 6(a) and (b)), we cannot compare the width of active zone quantitatively. The width of the ^{18}O peaks seems to be wider in Au than that in $La_{0.9}Sr_{0.1}MnO_3$ at the TPB region. This does not always represent the real widths of the active zone for oxygen incorporation. However, we can identify that the TPB is the most active site for oxygen incorporation, and inward ^{18}O diffusion in the mesh is preferable at the $La_{0.9}Sr_{0.1}MnO_3$-mesh/YSZ interfaces.

3.5. Active zone expansion around the TPB

The present SIMS imaging analysis clearly showed the difference in the distribution of oxygen incorporation active sites at the cathode/YSZ interfaces (Au and $La_{0.9}Sr_{0.1}MnO_3$). The expansion of the effective oxygen incorporation sites from the TPB line can be observed, especially in the $La_{0.9}Sr_{0.1}MnO_3$-mesh. The expansion of the active sites is mainly due to the following two factors: (1) bulk diffusion of oxygen through the cathode materials; and (2) high diffusivity of oxygen at the cathode/YSZ interfaces. Fig. 8 shows a schematic representation of oxygen reduction and equal potential lines of oxygen (broken lines) inside the cathode/electrolyte interfaces. With respect to the factor (1), we have already reported the bulk diffusion of oxygen in the dense $LaMnO_3$ film under the cathodic polarization [28]. The higher cathodic overpotential reduces the oxygen potential at the TPB and eventually it enhances the bulk diffusion of oxygen in the $LaMnO_3$ film. Therefore, the bulk oxygen diffusion in the cathode as shown in Fig. 8 (or, path of (4) in Fig. 1) can affect the distribution of ^{18}O on YSZ surface in the case of $La_{0.9}Sr_{0.1}MnO_3$-mesh. In this experimental condition, the cathodic overpotential (-0.33 V versus

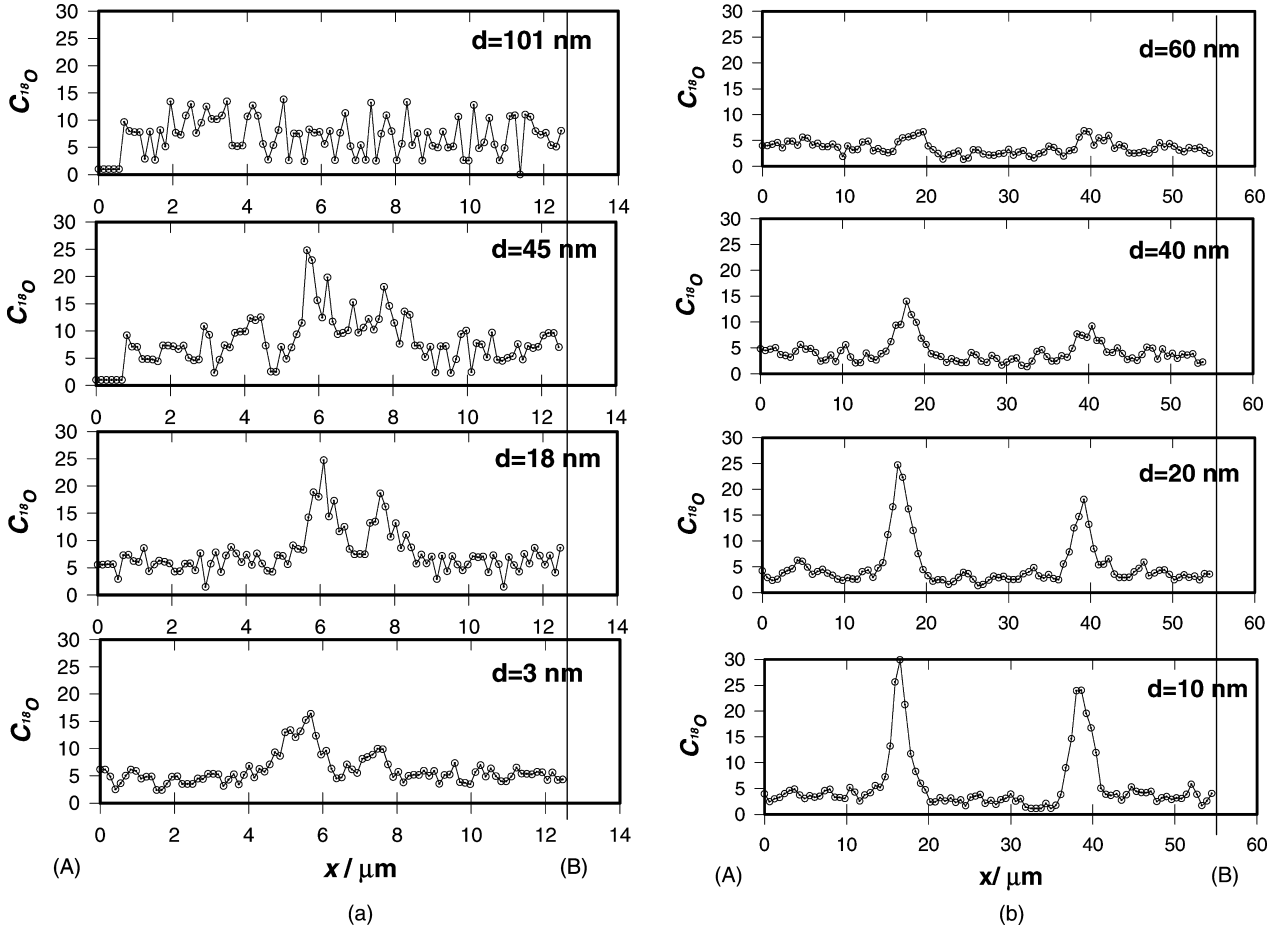

Fig. 7. Line analyses of the SIMS images of the YSZ surfaces at different depths: (a) $La_{0.9}Sr_{0.1}MnO_3$-mesh removed YSZ surface; (b) Au-mesh removed YSZ surface. $C^{18}O = I(180)/\{I(180) + I(160)\}^{*}1000$.

0.1 bar of oxygen partial pressure at 973 K) gives the oxygen partial pressure of 9×10^{-9} bar at the TPB. This low oxygen partial pressure can introduce the oxygen vacancies in the $La_{0.9}Sr_{0.1}MnO_3$-mesh and enhance bulk oxygen diffusion. Due to low diffusivity or low solubility of oxygen in the Au-mesh, high ^{18}O concentration is limited to the TPB lines with a low ^{18}O concentration at the Au-mesh/YSZ interface. About the factor (2), the expansion of the TPB zone is directly correlated with the interface diffusivity at the cathode/YSZ. In the case of $La_{0.9}Sr_{0.1}MnO_3$-mesh/YSZ, diffusion into the inside of the mesh is obviously observed. This suggests that the interface of $La_{0.9}Sr_{0.1}MnO_3$-mesh/YSZ is active for the interface diffusion of oxygen, which is completely different from the Au/YSZ interface.

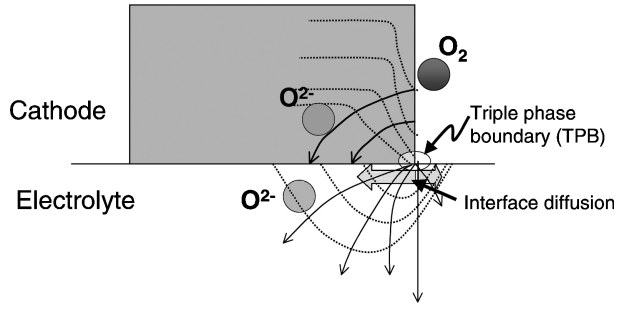

Fig. 8. Schematic drawing of the oxygen transport of oxygen and equivalent oxygen potential lines (broken lines) inside cathode and electrolyte materials.

Some authors previously analyzed the expansion of the active zone at the cathode/electrolyte interface based on electrochemical measurements. F.H. van Heuveln et al. [13] reported that the TPB zone width was less than 0.05 μm (50 nm) at 945 °C for the $La_{0.85}Sr_{0.15}MnO_3$/YSZ interfaces. The value is expected to be even smaller when the temperature is reduced, and it is quite small compared with the present SIMS images. A relatively thick width of the active zone for oxygen incorporation in the SIMS images suggests that SIMS images include oxygen diffusion in the YSZ near surface. This oxygen diffusion must affect the distribution of $^{18}O^{-}$ images from the TPB lines. The active zone for oxygen incorporation seems to expand inside the mesh as shown in Figs. 6 and 8. Recently, a numerical calculation of the cathode/electrolyte interface suggested that the cathode activity was proportional to the area of the contact between cathode and electrolyte [29]. This result supports our SIMS

observation and suggests the importance of the cathode/electrolyte interface properties.

4. Conclusions

The oxygen transport was visualized around the O_2/cathode/electrolyte TPBs by the $^{16}O/^{18}O$ exchange techniques and SIMS analysis. Higher ^{18}O concentration was observed on the $La_{0.85}Sr_{0.15}MnO_3$-mesh and the Au-mesh top surfaces, which suggested the promotion of oxygen adsorption and surface oxygen exchange on the mesh cathodes. Oxygen diffusion through the bulk of the cathode occurred only at the $La_{0.85}Sr_{0.15}MnO_3$-mesh, not at the Au-mesh. After removing the $La_{0.85}Sr_{0.15}MnO_3$-mesh, the active sites for oxygen incorporation were distributed in the shape of the mesh on the YSZ surface. This indicates that the $La_{0.85}Sr_{0.15}MnO_3$/YSZ interface is active for oxygen incorporation. On the other hand, in the case of Au-mesh removed YSZ surface, high ^{18}O concentration is observed only at the TPB region, which suggested the limitation of oxygen incorporation at the TPB. The line analysis of the SIMS images suggested that the most active sites for oxygen incorporation were at the TPB. The expansion of the active sites for oxygen incorporation was less than 1 μm from the TPB for both mesh cathodes. The active sites for oxygen incorporation are related to the bulk oxygen diffusion through the cathodes and the interface nature of cathodes/YSZ.

References

[1] B.A. van Hassel, B.A. Boukamp, A.J. Burggraaf, Solid State Ionics 48 (1991) 139.
[2] B.A. van Hassel, B.A. Boukamp, A.J. Burggraaf, Solid State Ionics 48 (1991) 155.
[3] Y. Takeda, R. Kanno, Y. Tomida, O. Yamamoto, J. Electrochem. Soc. 134 (1987) 2656.
[4] K. Tsuneyoshi, K. Mori, A. Sawata, J. Mizusaki, H. Tagawa, Solid State Ionics 35 (1989) 263.
[5] J. Mizusaki, H. Tagawa, K. Tsuneyoshi, A. Sawata, J. Electrochem. Soc. 138 (1991) 1867.
[6] J.A. van Roosemalen, E.H.P. Cordfunke, J. Solid State Chem. 93 (1991) 212.
[7] M. Kleitz, F. Petitbon, Solid State Ionics 92 (1996) 65.
[8] A. Hammouche, E. Siebert, A. Hammou, M. Kleitz, J. Electrochem. Soc. 138 (1991) 1212.
[9] E. Siebert, A. Hammouche, M. Kleitz, Electrochim. Acta 40 (11) (1995) 1741.
[10] R. Baker, J. Guindet, M. Keitz, J. Electrochem. Soc. 144 (1997) 2427.
[11] R. Jimménez, T. Kloidt, M. Kleitz, J. Electrochem. Soc. 144 (1997) 582.
[12] J. Van herle, A.J. McEvoy, K.R. Thanmpi, Electrochim. Acta 41 (1996) 1447.
[13] F.H. van Heuveln, H.J.M. Bouwmeester, F.P.F. van Berkel, J. Electrochem. Soc. 144 (1) (1996) 126.
[14] F.H. van Heuveln, H.J.M. Bouwmeester, F.P.F. van Berkel, J. Electrochem. Soc. 144 (1) (1996) 134.
[15] K. Sasaki, J.-P. Wurth, R. Gschwend, M. Gödickemeier, L.J. Gauckler, J. Electrochem. Soc. 143 (2) (1996) 530.
[16] C. Schwandt, W. Weppner, J. Electrochem. Soc. 144 (1997) 582.
[17] B. Gharbage, T. Pagnier, A. Hammou, J. Electrochem. Soc. 141 (8) (1994) 2118.
[18] H.Y. Lee, W.S. Cho, S.M. Oh, H.-D. Wiemhöfer, W. Göpel, J. Electrochem. Soc. 142 (8) (1995) 2659.
[19] A.M. Svensson, S. Sunde, K. Nisancioglu, J. Electrochem. Soc. 145 (4) (1998) 1390.
[20] Y. Jiang, S. Wang, Y. Zhang, J. Yan, W. Li, J. Electrochem. Soc. 145 (2) (1998) 373.
[21] A. Mittedorferm, L.J. Gauckler, Solid State Ionics 111 (1998)185.
[22] J. Mizusaki, T. Saito, H. Tagawa, J. Electrochem. Soc. 143 (10) (1996) 3065.
[23] J.A. Kilner, R.A. De Souza, I.C. Fullarton, Solid State Ionics 86-88 (1996) 703.
[24] T. Kawada, T. Horita, N. Sakai, H. Yokokawa, M. Doliya, J. Mizusaki, Solid State Ionics 131 (2000) 199.
[25] T. Horita, K. Yamaji, M. Ishikawa, N. Sakai, H. Yokokawa, T. Kawada, T. Kato, J. Electrochem. Soc. 145 (9) (1998) 3196.
[26] T. Horita, K. Yamaji, N. Sakai, H. Yokokawa, T. Kawada, T. Kato, Solid State Ionics 127 (2000) 55.
[27] T. Horita, K. Yamaji, H. Negishi, N. Sakai, H. Yokokawa, Electrochemistry (former Denki Kagaku) 68 (6) (2000) 433.
[28] T. Horita, K. Yamaji, N. Sakai, H. Yokokawa, T. Kawada, J. Electrochem. Soc. 148 (2001) J25.
[29] J. Fleig, J. Maier, in: S. C. Singhal, H. Yokokawa, (Eds.), Solid Oxide Fuel Cells, Vol. 7, PV2001-16, The Electrochemical Society, Pennington, NJ, USA, 2001, p. 583.